Published in final edited form as:
Skeletal Radiol. 2012 January ; 41(1): 15–31. doi:10.1007/s00256-011-1143-1.

High resolution imaging of tunnels by magnetic resonance neurography

Ty K. Subhawong,
The Russell H. Morgan Department of Radiology and Radiological Science, The Johns Hopkins Hospital, 601 N. Caroline Street, Room 4214, Baltimore, MD 21287, USA, tsubhaw1@jhmi.edu

Kenneth C. Wang,
Department of Radiology, Baltimore VA Medical Center, 10 North Greene Street, Baltimore, MD 21201, USA

Shrey K. Thawait,
The Russell H. Morgan Department of Radiology and Radiological Science, The Johns Hopkins Hospital, 601 N. Caroline Street, Room 4214, Baltimore, MD 21287, USA

Eric H. Williams,
Dellon Institute for Peripheral Nerve Surgery, 1122 Kenilworth Dr., #18, Towson, MD 21204, USA

Shahreyar Shar Hashemi,
Division of Plastic and Reconstructive Surgery, The Johns Hopkins Hospital, 601 N. Caroline Street, Baltimore, MD 21287, USA

Antonio J. Machado,
The Russell H. Morgan Department of Radiology and Radiological Science, The Johns Hopkins Hospital, 601 N. Caroline Street, Room 4214, Baltimore, MD 21287, USA

John A. Carrino, and
The Russell H. Morgan Department of Radiology and Radiological Science, The Johns Hopkins Hospital, 601 N. Caroline Street, Room 4214, Baltimore, MD 21287, USA

Avneesh Chhabra
The Russell H. Morgan Department of Radiology and Radiological Science, The Johns Hopkins Hospital, 601 N. Caroline Street, Room 4214, Baltimore, MD 21287, USA

Abstract

Peripheral nerves often traverse confined fibro-osseous and fibro-muscular tunnels in the extremities, where they are particularly vulnerable to entrapment and compressive neuropathy. This gives rise to various tunnel syndromes, characterized by distinct patterns of muscular weakness and sensory deficits. This article focuses on several upper and lower extremity tunnels, in which direct visualization of the normal and abnormal nerve in question is possible with high resolution 3T MR neurography (MRN). MRN can also serve as a useful adjunct to clinical and electrophysiologic exams by discriminating adhesive lesions (perineural scar) from compressive lesions (such as tumor, ganglion, hypertrophic callous, or anomalous muscles) responsible for symptoms, thereby guiding appropriate treatment.

Correspondence to: Ty K. Subhawong.

Conflict of interest The authors report no conflicts of interest.

Keywords

MRI; MR neurography; Peripheral nerve; Tunnels; 3T

Introduction

Peripheral nerve injuries and entrapments constitute a significant source of morbidity in the U.S. and European populations, resulting in more than 100,000 surgical procedures by some estimates [1]. The current reference standard for the evaluation of these lesions is clinical exam supplemented by electrophysiologic (EP) studies, such as electromyography (EMG), nerve conduction studies, and quantitative neurosensory testing. However, EP studies are invasive and provide only limited detail about the precise location and etiology of nerve injury and entrapment; moreover, an EP study may not be possible due to skin disorders; its results may be affected by patient's age, temperature, and body habitus; or the study may produce indeterminate results due to deeply situated nerves or underlying laboratory abnormalities (e.g., in serum Ca, K, or Mg) or medications [2, 3]. Consequently, there has been much interest in development and exploitation of MR imaging techniques capable of more precisely delineating nerve pathology and its underlying cause [4-6]. With technological advances in 3T MRI, MR neurography (MRN) is capable of generating high resolution and high contrast images of peripheral nerves, making it ideal for pre-surgical evaluation of suspected peripheral neuropathies [7, 8]. MRN allows both direct assessment of the nerve lesion, as well as indirect signs of nerve injury such as associated regional muscle denervation. MRN is particularly helpful in assessing nerves as they traverse confined spaces and tunnels, where they are susceptible to injury [2], providing better anatomic localization of the entrapment site than is possible with EMG studies, as well as information on the nature of the underlying causative lesion (e.g., benign or malignant mass, fibrosis, trauma). This article will focus on the MRN appearances of entrapped and/or injured nerves in various upper and lower extremity tunnels with relevant surgical correlations.

MRN technique

Historically, there have been two different types of MR techniques utilized in peripheral nerve imaging: diffusion-based and T2-based imaging [9, 10]. Using diffusion-based imaging, some investigators have found lowered fractional anisotropy values in nerve compression injuries such as carpal tunnel syndrome, believed to be due to widening of the interstitial space, Wallerian degeneration, and axonal demyelination, all of which contribute to an increased perpendicular diffusion vector compared to normal peripheral nerves [11, 12]. While diffusion-weighted sequences offer the potential for nerve tractography, current limitations in spatial resolution, required technical skill, and interpretation difficulties have prevented more widespread clinical implementation.

Advantages of T2-based imaging include relative simplicity of protocol design and execution, reproducibility, proven validity, and familiarity to clinical radiologists [8, 9, 13]. T2 weighting enhances the conspicuity of low-protein endoneurial fluid around the axons confined by the perineural blood/nerve barrier [14] (Fig. 1). Utilizing a combination of high resolution T1W images and high resolution as well as high contrast fat suppressed T2W images in the axial plane perpendicular to the long axis of the nerve is essential for detailed demonstration of peripheral nerve anatomy, fascicular morphology, and nerve pathology. Short-tau inversion recovery (STIR) generally outperforms frequency selective fat saturation with respect to homogeneity of signal suppression. Spectral adiabatic inversion recovery (SPAIR, Siemens, Erlangen, Germany) is the preferred T2W sequence on 3T as it is capable

of providing better signal to noise ratio (SNR) compared to STIR sequence and is also less sensitive to field heterogeneity than frequency selective fat saturation [15].

A third, novel hybrid approach utilizing elements of both diffusion weighting and T2 weighting is diffusion weighted three-dimensional DW-PSIF sequence (diffusion weighted reversed fast imaging with steady-state free precession) (Table 1). This sequence has shown promise in depicting cranial nerves [16], and in our initial experience, provides easy visualization of peripheral nerves in the extremities due to the selective suppression of vascular flow (Fig. 2).

Axial planes are generally best for the evaluation of abnormal T2 hyperintensity of the nerve (approaching the T2 SI of the adjacent vessels), individual fascicular abnormality, and relationship of nerve to the fibrosis or mass lesions. The findings are confirmed on coronal and sagittal planes to avoid the pitfall of artifactually increased T2 signal intensity (SI) from magic angle phenomenon [17]. Higher field strength (3T) magnets offer the possibility of acquiring 3D data sets with isotropic voxel resolution, and sequences such as 3D T2W SPACE (sampling perfection with application optimized contrasts by using different flip angle evolutions, Siemens, Erlangen, Germany) and 3D STIR SPACE are particularly well suited to MRN. These high contrast and high resolution (0.4–1 mm in plane resolution) sequences not only have more favorable specific absorption rate (SAR) profiles, but also offer spin-echo type contrast and multiplanar reformatting at the radiologist's workstation, which is essential for assessment of smaller peripheral nerves that course through a variety of oblique planes. Reformatting along the long axis of the nerve in question helps evaluation of subtle contour abnormalities or nerve displacement [8, 18]. 3D acquisitions also allow the reconstruction of maximum-intensity projection images, which increase nerve conspicuity (Fig. 3). For the evaluation of post-operative complications (e.g., abscess, hematoma, neuritis) or known masses, 3D volumetric interpolate breath-hold exam (VIBE) is a useful post-contrast sequence with multiplanar capabilities. Normal nerves do not enhance due to the presence of the blood nerve barrier (Table 1). Post-traumatic neuromas also do not enhance as compared to nerve sheath tumors [8, 18]. Finally, an integrated, team approach involving the radiologist, referring clinicians, and MR technologist is optimal for execution of patient- and pathology-specific protocols, thereby addressing specific clinical concerns, such as the presence of proximal pathology that may be excluded on a routine smaller field of view.

Nerve anatomy

To understand the MRN findings in both normal and abnormal nerves, a brief review of nerve anatomy is helpful. The axon, which constitutes a single nerve fiber, is the functional unit of each peripheral nerve, supported by surrounding Schwann cells. A connective tissue layer, the endoneurium, surrounds each axon and its Schwann cells; multiple axons together form a nerve fascicle, which is covered by the perineurium. It is the perineurium that is primarily responsible for bearing tensile loads and maintenance of intrafascicular pressure. A group of fascicles together form the nerve, which is itself covered with a final layer of connective tissue, the epineurium. This outer layer also partially invests the fascicles and contains the supporting vasculature [19, 20].

MRN findings of normal and abnormal peripheral nerves

Normal nerves demonstrate a fascicular appearance with isointense to minimally hyperintense signal intensity to skeletal muscle on T2 SPAIR TSE and STIR sequences (see Fig. 1). The epineural fat should be seen as preserved plane of tissue surrounding the nerve. Finally, the anatomic course of nerves should be free of sharp or acute angulation. Abnormal

nerves show a combination of various abnormalities, such as focal or diffuse nerve enlargement (larger than adjacent arteries or contralateral nerve), T2 hyperintensity approaching the adjacent vessels, fascicular abnormality (enlargement, disruption, or effacement), course deviations or discontinuity or abnormal enhancement.

The peripheral nerve may get compressed or may get injured in various tunnels. A “tunnel” can be defined as a confined space through which a peripheral nerve normally passes, where it is particularly susceptible to various intrinsic or extrinsic abnormalities that may lead to nerve compression [2]. The most common injuries of the peripheral nerves can be considered to primarily involve either traction/shearing forces or extrinsic compression. Seddon established a grading pattern for traumatic traction/shearing injuries based on the nerve continuity: neurapraxia, axonotmesis, and neurotmesis [21]. Neurapraxia is the mildest injury, describes nerve injury without axonal disruption, and is usually transient with full recovery of nerve function. In axonotmesis, the axon is disrupted, but the integrity of the surrounding myelin sheath is left intact. More severe injuries in which there is disruption of both the axon and its surrounding myelin sheath are categorized as neurotmesis. If transected, the nerve’s attempt at regeneration may result in a neuroma, which consists of a bulbous swelling of disorganized fascicular proliferation and fibrous tissue [22]. Surgical intervention is generally reserved for neurotmesis and more severe cases of axonotmesis. MRN may demonstrate various grades of severity [14] but may not be specific enough to differentiate neurapraxia from milder forms of axonotmesis.

Peripheral neuropathy due to external compression depends upon the degree of pressure. Pressures of around 20 mm Hg cause reduction in venous supply to the nerve, around 40 mm Hg is required for reduction in arterial supply to the nerve, and irreversible structural damage begins at pressures around 80 mm Hg [23]. Compressed nerves display increasing abnormal T2 hyperintensity due to various hypothesized mechanisms, such as blocked axoplasmic flow, venous congestion, edema, ischemia, mechanical insult, and Wallerian degeneration [14, 19, 24]. Long-standing compression (>6 months) results in chronic inflammation and perineural fibrosis [23], which can be seen as a disruption in the normally smooth contour of the perineural fat plane, particularly on T1 sequences. These findings, often in conjunction with nerve swelling, angulation, or displacement, are characteristic of nerve entrapment.

Other important observations include the identification of fusiform swelling in the nerve tissue, which is suggestive of neuroma in continuity (NIC). Denervation muscle changes, as secondary findings, are appreciated by presence of an edema-like signal in acute/subacute nerve injury and muscle fatty replacement with atrophy in more chronic injury [25]. This article will focus on various important tunnels in the upper and lower extremities (Table 2).

Carpal tunnel

Median neuropathy due to entrapment within the carpal tunnel is the most common neuropathy of the upper extremity, with a prevalence of approximately 50 cases per 1,000 subjects [26]. The carpal tunnel is formed by the concave surface of the carpus and is covered by the flexor retinaculum. It contains the long flexor tendons of the fingers and thumb, and the median nerve. In the palm, the median nerve gives off sensory branches to the first, second, third digits and the radial half of the fourth digit as well as a radial motor branch, which supplies the thenar muscles [27]. Major reasons for impingement include median nerve compression during wrist flexion at the transverse carpal ligament, space-occupying lesions, synovitis at the hook of the hamate, tethering of the nerve due to scar tissue, occupation-related repetitive motion trauma, and idiopathic causes [28]. Symptoms can include nocturnal pain, hand weakness, and paresthesias in the median nerve

distribution. On clinical exam, Phalen's test (increased paresthesia after 1 min passive wrist flexion) and Tinel's sign (paresthesia in nerve territory after gentle tapping over carpal tunnel) are often positive. Although EP studies are commonly performed for wrist neuropathies, false negative rates are as high as 30% and positive predictive values as low as 33%, which clearly indicate a need for improved diagnosis [29]. MRI has been reported to be positive in over 90% of cases [30], and MR findings were recently shown to predict surgical benefit for patients with carpal tunnel syndrome independently of the nerve conduction studies [31]. However, isolated MR sign of abnormal nerve T2 hyperintensity has low reported specificities of <40%, and this has limited more widespread adoption of imaging for diagnosis of carpal tunnel syndrome (CTS) in the clinical setting [32]. Therefore, it becomes imperative to use other MRN signs of neuropathy, such as median nerve enlargement (>10 mm) proximal to the tunnel with distal flattening at the level of the hook of the hamate, or abnormality of the fascicles, in addition to abnormal increased T2 signal [30, 32]. Volar bowing of the retinaculum (Fig. 4), effacement of carpal tunnel fat planes, and thenar muscle denervation edema may be seen as other associated secondary findings of median nerve compression [29, 33]. Underlying causative lesions identifiable on MRI include tenosynovitis, ganglion, hematoma, lipoma, persistent median artery, or other space-occupying masses (Fig. 5), but most cases remain idiopathic [34]. 3T MRN allows identification of individual bundle abnormalities of a bifid nerve, and nerve abnormalities can also be depicted in the longitudinal plane of the nerve to facilitate communication with the referring physician. Finally, post-treatment response (return of normal median nerve size/signal) can be monitored, and successful release of the flexor retinaculum after surgery can be confirmed.

Guyon's canal

Guyon's canal (ulnar tunnel) is a fibro-osseous tunnel enclosing the ulnar nerve, artery, and veins. The pisiform bone forms the medial boundary along with the hook of the hamate. The palmar carpal ligament forms the roof of the canal, while the floor is composed of tendons of the flexor digitorum profundus, transverse carpal ligament, pisohamate and pisometacarpal ligament, and opponens digiti minimi. The two terminal branches of the nerve can be easily visualized: the sensory branch running in proximity to the ulnar artery, and the motor branch, which courses more deeply, adjacent to the medial surface of the hamate hook. Entrapment neuropathy due to extrinsic compression (e.g., bicycle handle bars) and a number of intrinsic space-occupying lesions (ganglion, lipoma, ulnar artery aneurysm, and anomalous muscle, such as accessory abductor digiti minimi) as well as chronic traction neuritis due to fractures or use of crutches have been described [2, 28, 32, 34]. The site of compression may be classified among three zonal locations [35]:

Zone 1: Proximal edge of palmar carpal ligament to bifurcation of ulnar nerve (deep motor and superficial sensory branches); combined motor and sensory deficits

Zone 2: From nerve bifurcation to just distal to fibrous arch of hypothenar muscles; pure motor deficit

Zone 3: Parallels zone 2, distal end of canal containing superficial sensory branch; pure sensory deficit

Lesions in zones 1 and 3 are the most common, although most patients have symptoms in more than one zone. MRI findings of ulnar neuropathy due to entrapment include abnormal size, enlarged fascicles, and abnormally increased T2 signal intensity of the ulnar nerve; additionally, secondary signs of neuropathy include denervation atrophy/edema of the hypothenar muscles, 3rd/4th lumbricals, and interossei muscles (Fig. 6). Isolated deep bundle neuritis may also be detected on high resolution 3T MRN, which is difficult to diagnose on EMG.

Cubital tunnel

The ulnar nerve is the sole structure of significance within the cubital tunnel, which is the second most common site of nerve entrapment in the upper extremity [2]. The floor of the tunnel is comprised of the elbow joint capsule, as well as posterior and transverse portions of the medial collateral ligament (MCL). Its roof is formed by the cubital tunnel retinaculum (Osborne ligament) proximally and by the deep fibers of the flexor carpi ulnaris aponeurosis (arcuate ligament) distally [36]. Increased tension along these distal fibers occurs during flexion, and if prolonged, can result in a compressive neuropathy (e.g., “cell phone neuritis”). Other causes of cubital tunnel narrowing include an anomalous anconeus epitrochlearis muscle (Fig. 7), MCL disease, thickened cubital tunnel retinaculum (i.e., Osborne lesion), and various space-occupying lesions (e.g., hetero-topic ossification, loose bodies, tumors, scarring, fracture fragments, and ganglion cysts) [28, 32, 34]. Symptoms include transient paresthesia in the ring/small fingers, which may be accompanied by intrinsic muscle atrophy, and pain, which can be localized over the cubital tunnel or radiate to the wrist or shoulder. Tinel’s sign over the cubital tunnel is often present.

Direct MRN findings of neuropathy include increased T2 signal of the nerve, enlarged fascicles, and nerve displacement and/or angulation. In addition, the underlying cause of nerve injury/entrapment may be apparent and muscle denervation edema, which, when present as a secondary sign of neuropathy, is seen in the flexor carpi ulnaris, flexor digitorum profundus of 4th and 5th fingers, hypothenar and interosseous muscles of hand. In fact, patients with cubital tunnel syndrome are more likely to present with muscle wasting than patients with carpal tunnel syndrome [37]. Additionally, MRN may be used to evaluate patients at risk for so-called double crush injuries, in which distal nerve injury increases the vulnerability of the proximal course of the nerve, particularly prevalent in cyclists [32, 38]. Surgical release of an entrapped nerve may involve subcutaneous or submuscular transposition anteriorly, in which case post-operative findings will show the ulnar nerve anterior to the medial humeral condyle (Fig. 8). Re-entrapment of the anteriorly transposed ulnar nerve may also occur due to overzealous dissection and development of perineural fibrosis, requiring repeat surgical ulnar nerve release. MRN findings in these cases may show persistent/increasing T2 SI within the nerve and/or enlarged nerve fascicles in the hyperemic re-entrapped ulnar nerve. Encasing perineural fibrosis and regional muscle denervation changes are also nicely depicted, thereby confirming the clinical findings. Additionally, disuse/post-operative muscle edema (usually focal with or without associated fascial edema) can be differentiated from denervation edema (diffuse and without fascial edema) [39].

Radial tunnel and PIN syndrome

The boundaries of the radial tunnel include the capitellum (posteriorly), the supinator muscle (anteriorly), the brachioradialis, extensor carpi radialis longus and brevis muscles (anterolaterally), and the brachialis muscle (medially). Its contents include the radial nerve, which divides in the proximal forearm into superficial (primarily sensory) and deep (primarily motor) branches. The superficial branch of the radial nerve descends in the forearm under the brachioradialis and eventually pierces the deep fascia near the back of the wrist. The deep branch of the radial nerve pierces the supinator muscle, after which it is known as the posterior interosseous nerve (PIN) [36]. Although radial neuropathy is the least common elbow neuropathy [40], variation in how different authors define the radial tunnel has led to the appearance of different names for radial neuropathies based on the site of compression (radial tunnel syndrome, PIN syndrome, supinator syndrome) [2]. Compression sites from proximal to distal include the following: fibrous bands from the radiocapitellar joint, the tendinous edge of the extensor carpi radialis brevis muscle, adjacent

to the radial recurrent artery and its branches (Leash of Henry), at the arcade of Frohse (tendinous proximal end of supinator), and a fibrous band at distal end of supinator muscle [2, 40].

Of these, entrapment of the posterior interosseous nerve beneath the arcade of Frohse (i.e., posterior interosseous neuropathy, PIN syndrome) is the most commonly encountered lesion. Thickening of the arcade of Frohse, which represents the tendinous continuation of the proximal superficial head of the supinator, may develop after repetitive pronation/supination microtrauma [2, 41]. Motor neuropathy is a hallmark feature of PIN syndrome (also known as supinator syndrome). In this injury, loss of ability to extend the digits as well as radial wrist deviation due to weakness of the extensor carpi ulnaris typifies clinical findings [36, 40]. It should also be noted that many cases of refractory “tennis elbow” (i.e., lateral epicondylitis) may in fact be due in part to posterior interosseous nerve entrapment, as there is clinical overlap in their presentation [42]. MRN findings include enlarged and abnormally T2 hyperintense radial nerve or posterior interosseous nerve with regional muscle denervation changes in extensor compartment muscles of forearm (Fig. 9). In our experience, it often becomes difficult to distinguish the posterior interosseous nerve from adjacent smaller veins in the mid-distal forearm, as the whole neurovascular bundle appears T2 hyperintense. Fortunately, the entrapment sites are usually in the proximal forearm and elbow area and the abnormal nerve can be differentiated from the vessels in most cases; nevertheless, it is still imperative to evaluate the extensor muscles in clinically suspected cases of PIN neuropathy, as denervation edema in these muscles is the most common MRI manifestation of the syndrome [43].

Radial tunnel syndrome, on the other hand, is a distinct clinical entity, often occurring as the result of repetitive motion injuries to the elbow, and distinguished by the general absence of motor weakness [44]. Patients typically report pain in the region of the proximal extensor and supinator muscles, exacerbated by forearm pronation, extension of the elbow, and flexion of the wrist [40, 45]. While ultrasound is currently the modality of choice for evaluating the superficial sensory branches responsible for these symptoms [46], technological advances in high-resolution MRI may allow MRN to play a diagnostic role in the future.

Anterior interosseous nerve

The anterior interosseous nerve (AIN) arises from the radial aspect of the median nerve, as it courses between the two heads of the pronator teres muscle. Compression neuropathy of the AIN (also known as Kiloh-Nevin syndrome) results in predominantly motor symptoms involving the flexor digitorum profundus, flexor pollicis longus, and pronator quadratus muscles. While direct trauma is the most common cause of AIN injury, anatomic causes of compression include fibrous bands from the deep (more common) or superficial head of the pronator teres to the brachialis fascia, variant course of the nerve running deep to both heads of the pronator teres, double lacertus fibrosus, accessory muscles, and an aberrant radial artery [32, 47, 48]. MRN may demonstrate the abnormal AIN between the flexor digitorum superficialis and profundus muscles as well as denervation changes of the flexor digitorum profundus, flexor pollicis longus, and the pronator quadratus (most common) muscles [32, 49, 50] (Fig. 10). The radiologist should be aware that other patterns of muscle edema in AIN injury (e.g., involvement of the flexor carpi radialis) may reflect variability in innervation [49] and that isolated increased signal in the pronator quadratus muscle is frequently unrelated to underlying nerve injury [51].

Suprascapular and spinoglenoid notches

Of the confined spaces about the shoulder containing nerves susceptible to entrapment, those encountered most commonly clinically involve the suprascapular nerve, at the suprascapular and spinoglenoid notches, and the axillary nerve within the quadrilateral space. Both of these nerves carry fibers originating from the C5 and C6 nerve roots. The suprascapular nerve arises from the trunk formed by the union of these two roots, while the axillary nerve arises more distally from the posterior cord. The suprascapular notch is a bony depression of the scapula, medial to the coracoid process, which is covered by the transverse scapular ligament. This fibro-osseous tunnel forms a fixed point through which the suprascapular nerve must pass, where it is vulnerable to entrapment due to mass lesions such as paralabral cysts, enlarged veins, variant ligaments and muscular insertions, retracted rotator cuff tears, and tumors [52-54]. The suprascapular nerve then passes posterolaterally across the supraspinatus fossa and then through the spinoglenoid notch, which lies approximately 2 cm medial to the glenoid rim. This notch is covered by the appropriately named spinoglenoid ligament and also comprises an anatomic site of potential nerve compression. While paralabral ganglion cysts and other space-occupying lesions are often responsible for entrapment at the spinoglenoid notch, this site is also susceptible to dynamic compression neuropathy as the spinoglenoid ligament becomes taut in the follow-through phase of throwing motion [52]. Because the suprascapular nerve carries both motor and sensory components, suprascapular neuropathy manifests as posterolateral and/or superior shoulder pain, with mild weakness in abduction and external rotation. Key MRI findings of suprascapular neuropathy include denervation edema of both the supraspinatus and infraspinatus muscles (Fig. 11) when entrapment is at the level of the suprascapular notch, and isolated infraspinatus denervation edema when entrapment occurs at the spinoglenoid notch (Fig. 12).

Quadrilateral space

The quadrilateral (or quadrangular) space is located in the posterior aspect of the upper arm and formed by the teres minor and major muscles, long head of the triceps muscle, and medial cortex of the proximal humerus. It contains both the axillary nerve as well as the posterior humeral circumflex artery. Paralabral cysts and fibrous bands have been reported as causes of nerve impingement within the space [55], as well as large humeral head osteophytes (Fig. 13), with resultant axillary neuropathy manifesting as shoulder pain and weakness in abduction. While selective neurogenic edema or atrophy of the teres minor muscle should prompt an assessment of the quadrilateral space for a space-occupying lesion, it is much more commonly the result of other mechanical shoulder injuries, such as rotator cuff pathology or axillary nerve traction injury [55, 56]. MRI can also reveal other causes of muscle weakness, such as Parsonage-Turner syndrome (viral peripheral neuritis/brachial plexitis), which may lead to a denervation pattern involving more than one nerve distribution.

Thoracic outlet syndrome

The thoracic outlet can be subdivided into three anatomic spaces, from medial to lateral: the interscalene triangle, the costoclavicular space, and the retropectoralis minor space (also called the subcoracoid tunnel) [57]. The interscalene triangle is bordered anteriorly by the anterior scalene muscle, posteriorly by both the middle and posterior scalene muscles, and inferiorly by the first rib. It contains the subclavian artery and the three trunks of the brachial plexus. The costoclavicular space is bounded anteriorly by the subclavius muscle, anterosuperiorly by the clavicle, and posteriorly by both the first rib and the middle scalene muscle. This space contains the subclavian artery and vein, as well as the three cords of the

brachial plexus. The most lateral portion of the thoracic outlet, the retropectoralis minor space, is defined by the pectoralis minor anteriorly, subscapularis muscle posteriorly and superiorly, and the anterior chest wall posteriorly and inferiorly. It contains the distal cords and, just lateral to the pectoralis minor, selected terminal branches of the brachial plexus including the median nerve, ulnar nerve, musculocutaneous nerve, axillary nerve, and radial nerve [57]. Axial T1W images are useful to detect asymmetry of the scalene muscles or variant intramuscular course of the nerves, and coronal STIR images best depict asymmetry of the nerve size and signal intensity compared to the normal contralateral side. In our experience, sagittal 2D STIR or 3D STIR SPACE MRN images are most useful as they allow the plexus to be viewed in cross-section and nicely define the relationship of the nerves to the surrounding soft tissues. Individual root, trunk, or cord abnormalities are manifested as asymmetrically increased size and T2 SI. Space-occupying lesions such as cervical ribs, fibrous bands, and anomalous muscles predispose to arterial and/or nerve compression, which is typically exacerbated by dynamic arm elevation. We do not routinely perform the exams with arms abducted (“superman position”) unless specified by the referring physician. Neuropathies are most frequently localized to the costoclavicular and interscalene spaces (Fig. 14) [58]. Wittenberg and Adkins identified post-radiation fibrosis and malignant involvement from breast and lung cancers as the most common causes of nontraumatic plexopathy [59]. Initial treatment consists of physical therapy and exercise programs aimed at reducing symptoms, with surgery reserved for conservative treatment failure. Surgical options are varied and while optimal strategies are still controversial, two popular techniques include supraclavicular exposure with scalenectomy and neuroplasty, and the transaxillary approach with first rib resection [60].

Soleal sling

While the tibial nerve is most commonly entrapped in the tarsal tunnel, more proximal entrapment sites are increasingly appreciated as a cause of tibial neuropathy. Mastalgia et al. first described entrapment of tibial nerve by the tendinous arch of origin of the soleus muscle in 1981 [61], referred to as the soleal sling. The fascial arch spanning its bipennate origin from the posterior aspect of the tibia and fibula forms the sling, which constitutes the roof over the tibial neurovascular bundle in a tunnel between the superficial and deep posterior compartments containing the tibialis posterior, flexor hallucis, and flexor digitorum longus muscles [62]. Symptoms of tibial nerve entrapment by the soleal sling include popliteal fossa and proximal calf pain, weakness of toe flexion, and sensory deficits in the foot that are aggravated by ambulation [63]. While there is little radiology literature regarding the MRN appearance of this particular neuropathy, our experience shows that direct visualization of the abnormally T2 hyperintense and flattened tibial nerve at the soleal sling with proximal nerve enlargement is possible with 3T MRI and dedicated MRN sequences. Secondary findings of gastrocnemius and soleus muscle denervation edema serve as other important findings (Fig. 15). These patients may benefit from soleal sling release [62].

Peroneal tunnel

The common peroneal nerve branches off the sciatic nerve at the level of mid to distal third of the thigh, and receives contributions from the L4-S1 nerve roots. As it courses distally, it lies superficially over the bony prominence of the fibular neck under the subcutaneous fascia, where it is vulnerable to compression as well as laceration and stretching injury [64]. It continues toward the anterior compartment of the lower leg, situated between the two heads of the peroneus longus and brevis muscles. Peroneal nerve injury constitutes one of the more common mononeuropathies in the lower extremities [65], due to its relatively fixed position at the fibular neck as it travels under the tendinous arch of the peroneus longus,

called the peroneal tunnel [66]. The nerve bifurcates at the level of the fibular neck into superficial and deep divisions. The deep peroneal nerve supplies motor innervation to the tibialis anterior, extensor digitorum longus and brevis, extensor hallucis longus, and sensory innervation to the first web space of the foot. The superficial component supplies motor innervation to the peroneus longus and brevis, and sensory innervation to the dorsal aspect of the foot.

Symptoms of common peroneal neuropathy thus reflect a combination of superficial and deep peroneal nerve compromise, including pain and paresthesia in the distribution of the nerve over the dorsum of the foot, and “foot drop” due to weakness in dorsiflexion. Various etiologies of peroneal neuropathy include extrinsic compression (e.g., from a plaster cast or postural traction during hip surgery), intraneural ganglion cysts, running injuries, severe ankle sprains, knee dislocation, and posterolateral corner injuries associated with cruciate ligament tears [2, 64, 67]. Central neurologic deficits that result in hypotonic foot drop may also produce secondary neuropathy due to excessive traction on the nerve [65].

MRN demonstrates abnormal common peroneal and deep peroneal nerves as enlarged and abnormally T2 hyperintense nerves, denervation edema of extensor compartment muscles, and may also show localized muscle strains of peroneal or lateral head gastrocnemius muscles confirming the site of injury (Fig. 16). After surgical release and neurolysis of the entrapped nerve, partial fibulectomy may be performed to reduce the risk of re-entrapment [64]. Despite the need for surgery in some patients, a recent prospective study of 49 patients with peroneal mononeuropathy showed good clinical outcomes with conservative rehabilitation therapy [68]. MR plays a key role in the diagnosis and pre-operative planning for patients with intraneural ganglion cysts of the peroneal nerve because successful surgical treatment of these lesions mandates that the cyst’s communication with the degenerative tibiofibular joint fluid is obliterated [69]. Failure to recognize and address this communication, which can also involve the tibial nerve, can result in post-operative recurrence [70].

Tarsal tunnel

The tarsal tunnel is a fibro-osseous tunnel, with its floor formed by the medial malleolus and the roof formed by the flexor retinaculum. In addition to the tibial nerve, the tunnel contains the long flexor tendons, such as tibialis posterior, flexor digitorum longus, and flexor hallucis longus, as well as the tibial artery and accompanying veins. The first branch of the tibial nerve at the ankle is the medial calcaneal nerve, which may originate proximal to the tarsal tunnel in up to 40% of patients; if such is the case, sensory deficits due to tarsal tunnel entrapment will spare the heel [71]. The tibial nerve then branches into the medial and lateral plantar nerves. The medial plantar nerve (MPN) innervates the abductor hallucis, flexor hallucis brevis, flexor digitorum brevis, and the first lumbrical muscles; the lateral plantar nerve (LPN) innervates the remaining muscles in the lateral aspect of the foot, including the abductor digiti quinti, abductor hallucis, quadratus plantae, interosseous muscles, and 2nd to 5th lumbricals [71]. Typically, bifurcation of the tibial nerve into the MPN and LPN occurs beneath the flexor retinaculum, forming two distinct tunnels separated by a fibrous septum through which the MPN and LPN pass, respectively (Fig. 17). When the calcaneal nerve tunnel is considered, there are then actually four medial ankle tunnels that comprise pathological sites of entrapment under the more general clinical diagnosis of tarsal tunnel syndrome [23].

Common points of entrapment for the MPN and LPN include the space between the abductor hallucis and quadratus plantae muscles, medial arch beneath the talus and navicular bones, and beneath the fascial sling [72]. Repetitive microtrauma from running can lead to

medial plantar nerve entrapment between the abductor hallucis muscle and a thickened master Knot of Henry (tendinous crossover between the flexor hallucis longus and flexor digitorum longus) in what has been termed jogger's foot. Entrapment of the first branch of the LPN, the inferior calcaneal nerve, may occur between the quadratus plantae and abductor hallucis muscles, particularly in cases of plantar fasciitis, and is known as Baxter's neuropathy; isolated denervation of the abductor digiti quinti muscle could suggest the diagnosis [73].

All of these nerves can become entrapped due to overuse injuries, improper footwear, or various space-occupying lesions such as ganglions, tendon sheath cysts, anomalous muscles, varicosities, bony spurs, and post-traumatic fibrosis [72-74]. Symptoms may include dysesthesia of the foot, worse at night or exacerbated by ambulation, pain radiating either distally or proximally from the medial ankle, and weakness in the muscle groups listed above [74]. Tinel's sign is frequently positive in cases of tarsal tunnel syndrome. In the authors' experience, isolated mild T2 hyperintensity of the medial plantar nerve as compared to skeletal muscle is frequently observed during routine evaluation of deranged ankle MRI examinations, likely reflecting subclinical traction/friction neuritis. Therefore, other signs of neuropathy, such as enlarged nerve or fascicles, encasing perineural fibrosis and denervation muscle changes should also be assessed before making the diagnosis of tarsal tunnel syndrome. In addition to the evaluation of nerve signal and morphology abnormalities in patients referred for initial work-up, MRN has been used in the post-operative setting to evaluate the etiology of failed surgical decompression. MRN may show incomplete surgical release of the retinaculum, which is an important factor to consider in the 10–20% of patients who fail initial surgery [75]. MRN may also confirm incomplete decompression by demonstrating various findings such as persistent tibial, MPN, and LPN abnormalities, encasing perineural fibrosis, neuroma in continuity formation, and persistent muscle denervation changes.

Morton's neuroma

Morton's neuroma, also called intermetatarsal neuroma, classically affects the third and less commonly, second and first intermetatarsal spaces. While "neuroma" may be a misnomer for this lesion given that it is not believed to represent a neoplasm, our use of this term follows convention. This neuroma is the result of entrapment in the confined space deep to intermetatarsal ligament and is characterized by chronic friction related perineural fibrosis, nerve degeneration, leukocyte infiltration, and epineural and endoneural vascular hyalinization, all of which further contribute to abnormal thickening of the nerve [76]. At the level of the metatarsal heads, the interdigital nerves, which are terminal branches of the medial and lateral plantar nerves, are cushioned by fat bodies. These fat cushions, along with the neurovascular bundles, are roofed by the deep transverse metatarsal ligament [77, 78]. Although the exact pathophysiology remains unclear, the increased incidence of Morton's neuroma at the third interdigital space may be related to fusion of branches from the medial and lateral plantar nerves in addition to compression from the superficial and deep transverse metatarsal ligaments or vascular etiologies [79]. Typical clinical complaints include sharp pain and burning in the region of the intermetatarsal space, as well as paresthesias exacerbated by weight bearing. Zanetti and Weishaupt outlined suggestive MRI findings of Morton's neuroma, including a well-defined spindle-shaped mass on the plantar side of the deep transverse metatarsal ligament near the neurovascular bundle, a caliber change of the nerve when viewed in a transverse plane, and abnormal signal intensity (Fig. 18) [77]. Conspicuity has been reported to be higher with prone positioning, possibly because increased flexion of the metatarsophalangeal joint pulls the neurovascular bundle with the Morton neuroma deeper into the intermetatarsal space [80]. Incidental neuromas, i.e., those that do not cause symptoms, are typically less than 5 mm in diameter [76].

Although early studies suggested that more than half of MR examinations may alter the clinical treatment plan [81], the role for imaging (MRI or ultrasound) remains controversial [79]. While contrast may not be required in general [77], in our experience it is particularly useful in the post-operative setting for detection of residual neuroma.

Conclusion

Novel pulse sequences on 3T MRI along with recent improvements in gradient and coil design allow MR neurography to play an expanding role in high-resolution evaluation of patients with peripheral neuropathy. MRN complements information gained from the current reference standard of clinical and EP studies. Its ability to directly demonstrate nerve abnormality, associated secondary regional muscle denervation changes, as well as the nature and location of underlying entrapment may allow more targeted therapeutic strategies and enhance presurgical planning.

Acknowledgments

This work was supported by grant number 1T32EB006351 from the NIH. Its contents are solely the responsibility of the authors and do not necessarily represent the official views of the NIH. K.C.W. gratefully acknowledges the support of RSNA Research and Education Foundation Fellowship Training Grant #FT0904, as well as that of the Walter and Mary Ciceric Research Award. A.C. acknowledges GERRAF, Siemens, and Integra Life Sciences research grants.

References

1. Siemionow M, Brzezicki G. Chapter 8: current techniques and concepts in peripheral nerve repair. Int Rev Neurobiol. 2009; 87:141–72. [PubMed: 19682637]
2. Pećina, M.; Krmpotić-Nemanić, J.; Markiewitz, AD. Tunnel syndromes. 3. Boca Raton: CRC Press; 2001.
3. Gutmann L. Pearls and pitfalls in the use of electromyography and nerve conduction studies. Semin Neurol. 2003; 23:77–82. [PubMed: 12870108]
4. Bashir WA, Connell DA. Imaging of entrapment and compressive neuropathies. Semin Musculoskelet Radiol. 2008; 12:170–81. [PubMed: 18509796]
5. Spratt JD, Stanley AJ, Grainger AJ, Hide IG, Campbell RSD. The role of diagnostic radiology in compressive and entrapment neuropathies. Eur Radiol. 2002; 12:2352–64. [PubMed: 12195495]
6. Filler AG, Howe FA, Hayes CE, et al. Magnetic resonance neurography. Lancet. 1993; 341:659–61. [PubMed: 8095572]
7. Stoll G, Bendszus M, Perez J, Pham M. Magnetic resonance imaging of the peripheral nervous system. J Neurol. 2009; 256:1043–51. [PubMed: 19252774]
8. Chhabra A, Williams EH, Wang KC, Dellon AL, Carrino JA. MR neurography of neuromas related to nerve injury and entrapment with surgical correlation. AJNR Am J Neuroradiol. 2010; 31:1363–8. [PubMed: 20133388]
9. Du R, Auguste KI, Chin CT, Engstrom JW, Weinstein PR. Magnetic resonance neurography for the evaluation of peripheral nerve, brachial plexus, and nerve root disorders. J Neurosurg. 2010; 112:362–71. [PubMed: 19663545]
10. Takahara T, Hendrikse J, Yamashita T, et al. Diffusion-weighted MR neurography of the brachial plexus: feasibility study. Radiology. 2008; 249:653–60. [PubMed: 18796657]
11. Andreisek G, White LM, Kassner A, Sussman MS. Evaluation of diffusion tensor imaging and fiber tractography of the median nerve: preliminary results on intrasubject variability and precision of measurements. AJR Am J Roentgenol. 2010; 194:W65–72. [PubMed: 20028893]
12. Khalil C, Budzik JF, Kermarrec E, Balbi V, Le Thuc V, Cotten A. Tractography of peripheral nerves and skeletal muscles. Eur J Radiol. 2010; 76:391–7. [PubMed: 20392583]
13. Bendszus M, Stoll G. Technology insight: visualizing peripheral nerve injury using MRI. Nat Clin Pract Neurol. 2005; 1:45–53. [PubMed: 16932491]

14. Filler AG, Maravilla KR, Tsuruda JS. MR neurography and muscle MR imaging for image diagnosis of disorders affecting the peripheral nerves and musculature. Neurol Clin. 2004; 22:643–82. vi–vii. [PubMed: 15207879]
15. Lauenstein TC, Sharma P, Hughes T, Heberlein K, Tudorascu D, Martin DR. Evaluation of optimized inversion-recovery fat-suppression techniques for T2-weighted abdominal MR imaging. J Magn Reson Imaging. 2008; 27:1448. [PubMed: 18504735]
16. Zhang Z, Meng Q, Chen Y, et al. 3-T imaging of the cranial nerves using three-dimensional reversed FISP with diffusion-weighted MR sequence. J Magn Reson Imaging. 2008; 27:454–8. [PubMed: 18219629]
17. Chappell KE, Robson MD, Stonebridge-Foster A, et al. Magic angle effects in MR neurography. AJNR Am J Neuroradiol. 2004; 25:431–40. [PubMed: 15037469]
18. Viallon M, Vargas MI, Jlassi H, Lovblad KO, Delavelle J. High-resolution and functional magnetic resonance imaging of the brachial plexus using an isotropic 3D T2 STIR (short term inversion recovery) SPACE sequence and diffusion tensor imaging. Eur Radiol. 2008; 18:1018–23. [PubMed: 18180925]
19. Geuna S, Raimondo S, Ronchi G, et al. Chapter 3: histology of the peripheral nerve and changes occurring during nerve regeneration. Int Rev Neurobiol. 2009; 87:27–46. [PubMed: 19682632]
20. Lee SK, Wolfe SW. Peripheral nerve injury and repair. J Am Acad Orthop Surg. 2000; 8:243–52. [PubMed: 10951113]
21. Seddon H. Three types of nerve injury. Brain. 1943; 66:237–88.
22. Vernadakis AJ, Koch H, Mackinnon SE. Management of neuromas. Clin Plast Surg. 2003; 30:247–68. vii. [PubMed: 12737355]
23. Dellon AL. The four medial ankle tunnels: a critical review of perceptions of tarsal tunnel syndrome and neuropathy. Neurosurg Clin N Am. 2008; 19:629–48. vii. [PubMed: 19010287]
24. Grant GA, Britz GW, Goodkin R, Jarvik JG, Maravilla K, Kliot M. The utility of magnetic resonance imaging in evaluating peripheral nerve disorders. Muscle Nerve. 2002; 25:314–31. [PubMed: 11870709]
25. Lisle DA, Johnstone SA. Usefulness of muscle denervation as an MRI sign of peripheral nerve pathology. Australas Radiol. 2007; 51:516–26. [PubMed: 17958685]
26. Bickel KD. Carpal tunnel syndrome. J Hand Surg Am. 2010; 35:147–52. [PubMed: 20117319]
27. Martinoli C, Bianchi S, Gandolfo N, Valle M, Simonetti S, Derchi LE. US of nerve entrapments in osteofibrous tunnels of the upper and lower limbs. Radiographics. 2000; 20 Spec No:S199–213; discussion S213–217.
28. Beltran J, Rosenberg ZS. Diagnosis of compressive and entrapment neuropathies of the upper extremity: value of MR imaging. AJR Am J Roentgenol. 1994; 163:525. [PubMed: 8079837]
29. Bordalo-Rodrigues M, Amin P, Rosenberg ZS. MR imaging of common entrapment neuropathies at the wrist. Magn Reson Imaging Clin N Am. 2004; 12:265–79. vi. [PubMed: 15172386]
30. Jarvik JG, Yuen E, Haynor DR, et al. MR nerve imaging in a prospective cohort of patients with suspected carpal tunnel syndrome. Neurology. 2002; 58:1597–602. [PubMed: 12058085]
31. Verdugo RJ, Salinas RA, Castillo JL, Cea JG. Surgical versus non-surgical treatment for carpal tunnel syndrome. Cochrane Database Syst Rev. 2008:CD001552. [PubMed: 18843618]
32. Andreisek G, Crook DW, Burg D, Marincek B, Weishaupt D. Peripheral neuropathies of the median, radial, and ulnar nerves: MR imaging features. Radiographics. 2006; 26:1267–87. [PubMed: 16973765]
33. Monagle K, Dai G, Chu A, Burnham RS, Snyder RE. Quantitative MR imaging of carpal tunnel syndrome. AJR Am J Roentgenol. 1999; 172:1581–6. [PubMed: 10350293]
34. Kim S, Choi J, Huh Y, et al. Role of magnetic resonance imaging in entrapment and compressive neuropathy—what, where, and how to see the peripheral nerves on the musculoskeletal magnetic resonance image: part 2. Upper extremity. Eur Radiol. 2007; 17:509–22. [PubMed: 16572333]
35. Stoller, DW.; Li, AE.; Lichtman, DW.; Brody, GA. Chapter 10: the wrist and hand. In: Stoller, DW., editor. MRI in orthopaedics and sports medicine. Baltimore, MD: Lippincott Williams & Wilkins; 2007. p. 1798-1802.

36. Bencardino, JT.; Rosenberg, ZS. Chapter 12: entrapment neuropathies of the upper extremity. In: Stoller, DW., editor. MRI in orthopaedics and sports medicine. Baltimore, MD: Lippincott Williams & Wilkins; 2007. p. 1946-1963.
37. Mallette P, Zhao M, Zurakowski D, Ring D. Muscle atrophy at diagnosis of carpal and cubital tunnel syndrome. J Hand Surg Am. 2007; 32:855–8. [PubMed: 17606066]
38. Smith TM, Sawyer SF, Sizer PS, Brismée JM. The double crush syndrome: a common occurrence in cyclists with ulnar nerve neuropathy—a case-control study. Clin J Sport Med. 2008; 18:55–61. [PubMed: 18185040]
39. May DA, Disler DG, Jones EA, Balkissoon AA, Manaster BJ. Abnormal signal intensity in skeletal muscle at MR imaging: patterns, pearls, and pitfalls. Radiographics. 2000; 20 Spec No: S295–315.
40. Bordalo-Rodrigues M, Rosenberg ZS. MR imaging of entrapment neuropathies at the elbow. Magn Reson Imaging Clin N Am. 2004; 12:247–63. vi. [PubMed: 15172385]
41. Miller TT, Reinus WR. Nerve entrapment syndromes of the elbow, forearm, and wrist. AJR Am J Roentgenol. 2010; 195:585–94. [PubMed: 20729434]
42. Wilhelm A. Tennis elbow: treatment of resistant cases by denervation. J Hand Surg Br. 1996; 21:523–33. [PubMed: 8856547]
43. Ferdinand BD, Rosenberg ZS, Schweitzer ME, et al. MR imaging features of radial tunnel syndrome: initial experience. Radiology. 2006; 240:161–8. [PubMed: 16793976]
44. Bolster MAJ, Bakker XR. Radial tunnel syndrome: emphasis on the superficial branch of the radial nerve. J Hand Surg Eur. 2009; 34:343–7.
45. Sarhadi NS, Korday SN, Bainbridge LC. Radial tunnel syndrome: diagnosis and management. J Hand Surg Br. 1998; 23:617–9. [PubMed: 9821607]
46. Stokvis A, Van Neck JW, Van Dijke CF, Van Wamel A, Coert JH. High-resolution ultrasonography of the cutaneous nerve branches in the hand and wrist. J Hand Surg Eur. 2009; 34:766–71.
47. Chin DH, Meals RA. Anterior interosseous nerve syndrome. J Hand Surg Am. 2001; 1:249–57.
48. Dang AC, Rodner CM. Unusual compression neuropathies of the forearm, part II: median nerve. J Hand Surg Am. 2009; 34:1915–20. [PubMed: 19969200]
49. Dunn AJ, Salonen DC, Anastakis DJ. MR imaging findings of anterior interosseous nerve lesions. Skeletal Radiol. 2007; 36:1155–62. [PubMed: 17938918]
50. Grainger AJ, Campbell RS, Stothard J. Anterior interosseous nerve syndrome: appearance at MR imaging in three cases. Radiology. 1998; 208:381–4. [PubMed: 9680563]
51. Gyftopoulos S, Rosenberg ZS, Petchprapa C. Increased MR signal intensity in the pronator quadratus muscle: does it always indicate anterior interosseous neuropathy? AJR Am J Roentgenol. 2010; 194:490–3. [PubMed: 20093614]
52. Piasecki DP, Romeo AA, Bach BR, Nicholson GP. Suprascapular neuropathy. J Am Acad Orthop Surg. 2009; 17:665–76. [PubMed: 19880677]
53. Fritz RC, Helms CA, Steinbach LS, Genant HK. Suprascapular nerve entrapment: evaluation with MR imaging. Radiology. 1992; 182:437–44. [PubMed: 1732962]
54. Carroll KW, Helms CA, Otte MT, Moellken SMC, Fritz R. Enlarged spinoglenoid notch veins causing suprascapular nerve compression. Skeletal Radiol. 2003; 32:72–7. [PubMed: 12589484]
55. Cothran RL, Helms C. Quadrilateral space syndrome: incidence of imaging findings in a population referred for MRI of the shoulder. AJR Am J Roentgenol. 2005; 184:989–92. [PubMed: 15728630]
56. Sofka CM, Lin J, Feinberg J, Potter HG. Teres minor denervation on routine magnetic resonance imaging of the shoulder. Skeletal Radiol. 2004; 33:514–8. [PubMed: 15221220]
57. Demondion X, Herbinet P, Van Sint Jan S, Boutry N, Chantelot C, Cotten A. Imaging assessment of thoracic outlet syndrome. Radiographics. 2006; 26:1735–50. [PubMed: 17102047]
58. Demondion X, Bacqueville E, Paul C, Duquesnoy B, Hachulla E, Cotten A. Thoracic outlet: assessment with MR imaging in asymptomatic and symptomatic populations. Radiology. 2003; 227:461–8. [PubMed: 12637678]

59. Wittenberg KH, Adkins MC. MR imaging of nontraumatic brachial plexopathies: frequency and spectrum of findings. Radiographics. 2000; 20:1023–32. [PubMed: 10903692]
60. Huang JH, Zager EL. Thoracic outlet syndrome. Neurosurgery. 2004; 55:897–902. discussion 902–903. [PubMed: 15458598]
61. Mastaglia FL, Venerys J, Stokes BA, Vaughan R. Compression of the tibial nerve by the tendinous arch of origin of the soleus muscle. Clin Exp Neurol. 1981; 18:81–5. [PubMed: 6926395]
62. Williams EH, Williams CG, Rosson GD, Dellon LA. Anatomic site for proximal tibial nerve compression: a cadaver study. Ann Plast Surg. 2009; 62:322–5. [PubMed: 19240533]
63. Mastaglia FL. Tibial nerve entrapment in the popliteal fossa. Muscle Nerve. 2000; 23:1883–6. [PubMed: 11102915]
64. Kim DH, Kline DG. Management and results of peroneal nerve lesions. Neurosurgery. 1996; 39:312–9. discussion 319–320. [PubMed: 8832668]
65. Tsur A. Common peroneal neuropathy in patients after first-time stroke. Isr Med Assoc J. 2007; 9:866–9. [PubMed: 18210927]
66. McCrory P, Bell S, Bradshaw C. Nerve entrapments of the lower leg, ankle and foot in sport. Sports Med. 2002; 32:371–91. [PubMed: 11980501]
67. Dellon AL. Postarthroplasty “palsy” and systemic neuropathy: a peripheral-nerve management algorithm. Ann Plast Surg. 2005; 55:638–42. [PubMed: 16327467]
68. Aprile I, Tonali P, Caliandro P, et al. Italian multicentre study of peroneal mononeuropathy: multiperspective follow-up. Neurol Sci. 2009; 30:37–44. [PubMed: 19153647]
69. Spinner RJ, Luthra G, Desy NM, Anderson ML, Amrami KK. The clock face guide to peroneal intraneural ganglia: critical “times” and sites for accurate diagnosis. Skeletal Radiol. 2008; 37:1091–9. [PubMed: 18641980]
70. Spinner RJ, Hébert-Blouin M, Maniker AH, Amrami KK. Clock face model applied to tibial intraneural ganglia in the popliteal fossa. Skeletal Radiol. 2009; 38:691–6. [PubMed: 19221739]
71. Oh SJ, Meyer RD. Entrapment neuropathies of the tibial (posterior tibial) nerve. Neurol Clin. 1999; 17:593–615. vii. [PubMed: 10393755]
72. Farooki S, Theodorou DJ, Sokoloff RM, Theodorou SJ, Trudell DJ, Resnick D. MRI of the medial and lateral plantar nerves. J Comput Assist Tomogr. 2001; 25:412–6. [PubMed: 11351192]
73. Delfaut EM, Demondion X, Bieganski A, Thiron M, Mestdagh H, Cotten A. Imaging of foot and ankle nerve entrapment syndromes: from well-demonstrated to unfamiliar sites. Radiographics. 2003; 23:613–23. [PubMed: 12740464]
74. McCluskey LF, Webb LB. Compression and entrapment neuropathies of the lower extremity. Clin Podiatr Med Surg. 1999; 16:97–125. vii. [PubMed: 9929774]
75. Zeiss J, Fenton P, Ebraheim N, Coombs RJ. Magnetic resonance imaging for ineffectual tarsal tunnel surgical treatment. Clin Orthop Relat Res. 1991:264–266. [PubMed: 1997244]
76. Bencardino J, Rosenberg ZS, Beltran J, Liu X, Marty-Delfaut E. Morton’s neuroma: is it always symptomatic? AJR Am J Roentgenol. 2000; 175:649–53. [PubMed: 10954445]
77. Zanetti M, Weishaupt D. MR imaging of the forefoot: Morton neuroma and differential diagnoses. Semin Musculoskelet Radiol. 2005; 9:175–86. [PubMed: 16247719]
78. Theumann NH, Pfirrmann CW, Chung CB, et al. Intermetatarsal spaces: analysis with MR bursography, anatomic correlation, and histopathology in cadavers. Radiology. 2001; 221:478–84. [PubMed: 11687693]
79. Sharp RJ, Wade CM, Hennessy MS, Saxby TS. The role of MRI and ultrasound imaging in Morton’s neuroma and the effect of size of lesion on symptoms. J Bone Joint Surg Br. 2003; 85:999–1005. [PubMed: 14516035]
80. Weishaupt D, Treiber K, Kundert H, et al. Morton neuroma: MR imaging in prone, supine, and upright weight-bearing body positions. Radiology. 2003; 226:849–56. [PubMed: 12601213]
81. Zanetti M, Strehle JK, Kundert HP, Zollinger H, Hodler J. Morton neuroma: effect of MR imaging findings on diagnostic thinking and therapeutic decisions. Radiology. 1999; 213:583–8. [PubMed: 10551246]

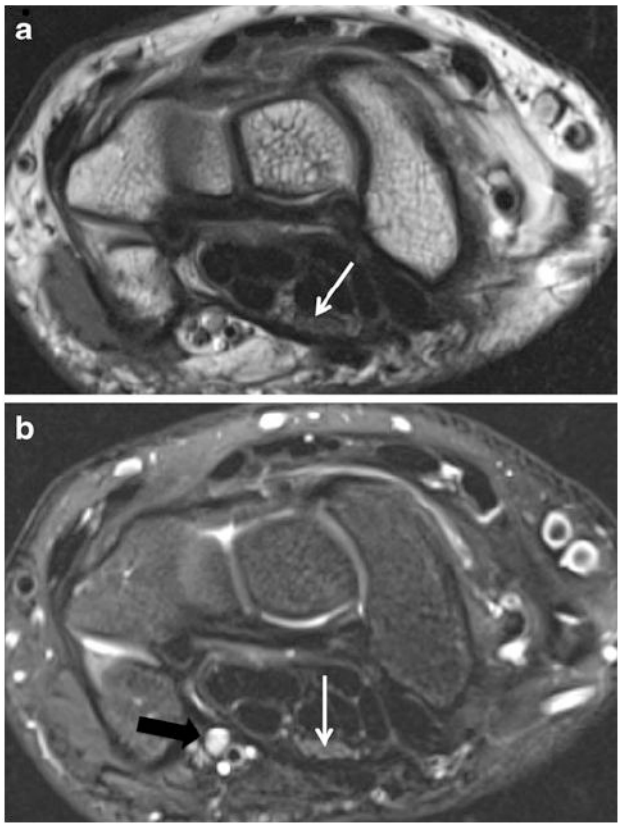

Fig. 1.
A 14-year-old boy with wrist pain. **a** Axial T1 image shows the normal fascicular pattern of the median nerve in the carpal tunnel (*arrow*), with well-preserved planes of surrounding perineural fat. **b** Axial T2 SPAIR image shows the normal intermediate signal intensity of the median nerve (*white arrow*), in contrast to the hyperintense vessels (*black arrow*)

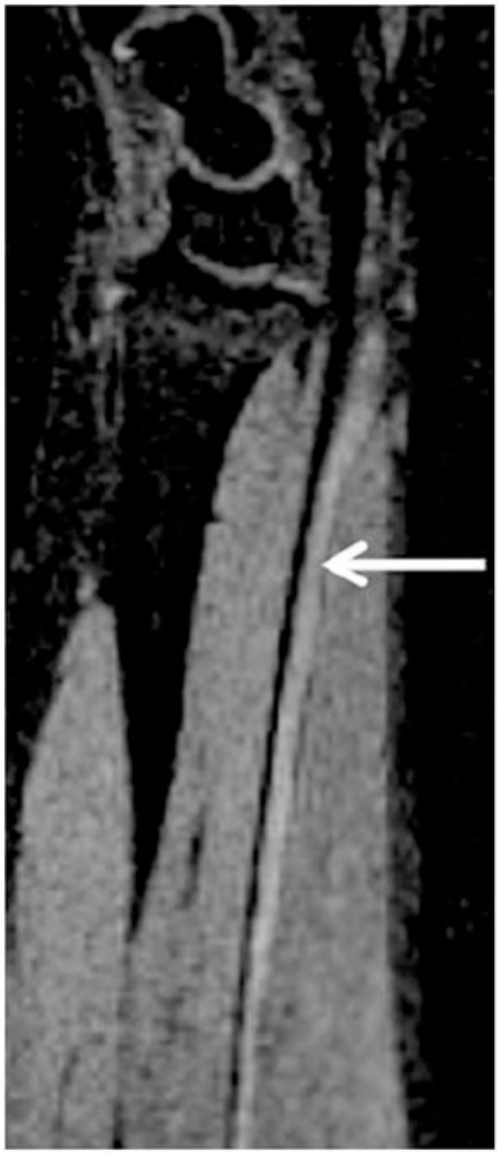

Fig. 2.
Sagittal PSIF (nerve selective) image demonstrates the normal course of the median nerve as it travels ventrally in the forearm

Fig. 3.
Coronal 3-D maximum intensity projection (MIP) from a STIR SPACE sequence of the brachial plexus demonstrates improved conspicuity of the nerve roots (*arrows*)

Fig. 4.

A 60-year-old man with left wrist pain due to carpal tunnel syndrome (idiopathic). Axial T2 SPAIR shows significant T2 hyperintensity and enlargement of the median nerve as well as contained fascicles (*arrow*), with minimal flexor tenosynovitis and volar bowing of the overlying flexor retinaculum (*arrowheads*)

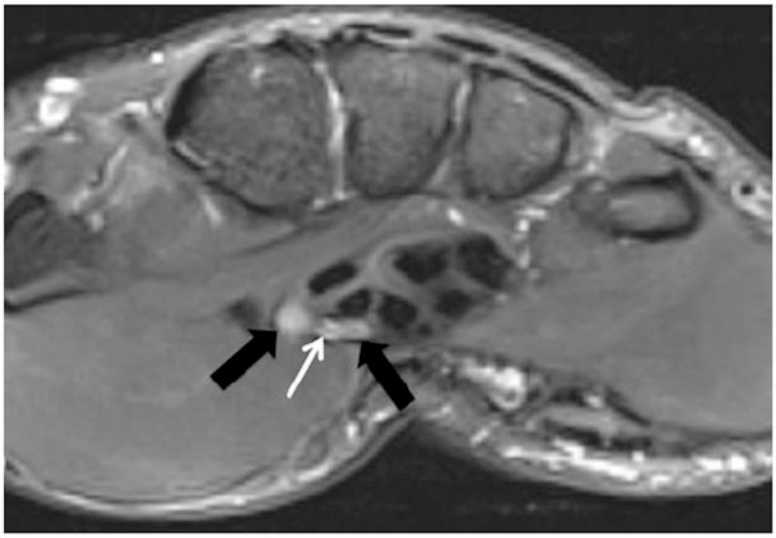

Fig. 5.

A 25-year-old man with history of trauma to right thumb and persistent pain. Axial T2 SPAIR images show a persistent median artery (*white arrow*) between the abnormally T2 hyperintense radial and ulnar bundles of the bifid median nerve (*black arrows*). A persistent median artery is a known cause of compression median neuropathy in the carpal tunnel

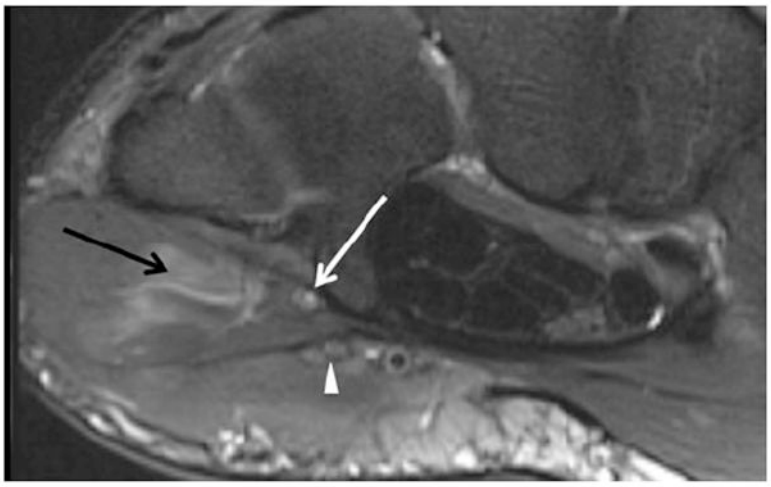

Fig. 6.

A 31-year-old male with ulnar sided wrist pain. Axial T2 SPAIR image just distal to Guyon's canal shows an isolated signal abnormality in the deep branch of the ulnar nerve (*white arrow*); note the associated denervation edema of the hypothenar muscles (*black arrow*). The more superficial branches are normal (*arrowhead*)

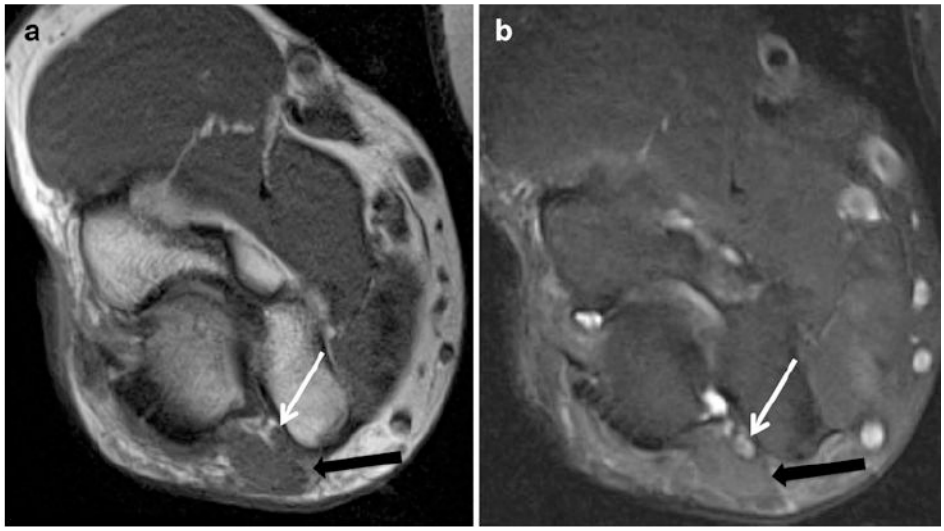

Fig. 7.
A 45-year-old man with history of forearm pain. **a** Axial T1 and **b** axial T2 SPAIR images show an accessory anconeus muscle (*black arrow*) causing compression and ulnar neuropathy (*white arrow*)

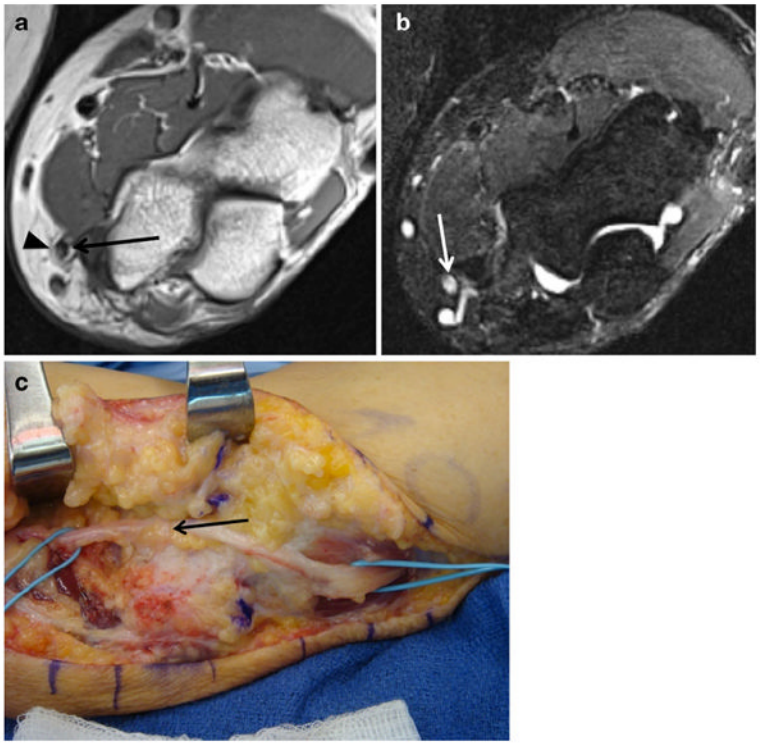

Fig. 8.
A 51-year-old male with persistent left upper arm pain as well as left hand pain and numbness, following prior surgical ulnar nerve transposition. **a** Axial T1 image demonstrates anterior subcutaneous position of the ulnar nerve (*arrow*). Note thin strand hypointense fibrotic bands (*arrowhead*) surrounding the nerve. **b** Axial T2 SPAIR shows abnormal hyperintensity of the ulnar nerve (*arrow*), approaching that of vessels. **c** Photograph from surgery shows the fibrous bands around the inflamed and hyperemic ulnar nerve (*arrow*), confirming the pre-operative MRI findings

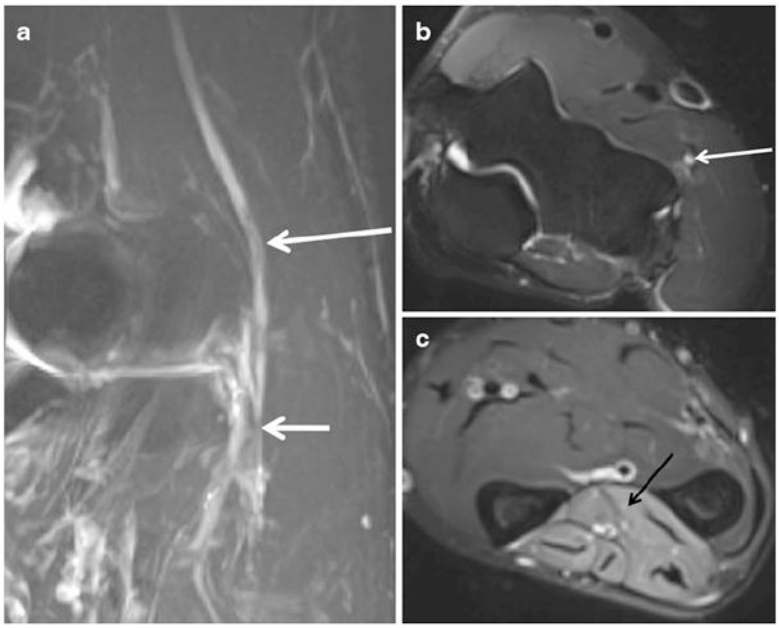

Fig. 9.

A 45-year-old man with elbow pain and weakness in finger extension. **a** Oblique coronal STIR MIP shows the abnormal radial nerve (*long arrow*), which is enlarged and hyperintense related to hypothesized mechanisms of blocked axoplasmic flow and venous congestion proximal to the site of entrapment at the arcade of Frohse (*short arrow*). **b** Axial T2 SPAIR image demonstrates the abnormal radial nerve, which shows abnormal hyperintense signal in the T2 weighted image (*white arrow*). **c** Axial T2 SPAIR more distally in the forearm shows extensive denervation edema-like signal affecting extensor compartment muscles (*black arrow*). MRI confirmed the clinical suspicion of posterior interosseous neuropathy and excluded the presence of any organic cause. The symptoms resolved on clinical follow-up

Fig. 10.

A 54-year-old with right thumb weakness and clinically suspected AIN neuropathy. **a** Axial T2 SPAIR shows high signal intensity (similar to vessels) of the AIN (*black arrow*). Axial T2 SPAIR images show denervation edema-like signal of the flexor digitorum profundus muscle (**b**, *thick white arrow*) as well as of the pronator quadratus muscle (**c**, *thin white arrow*)

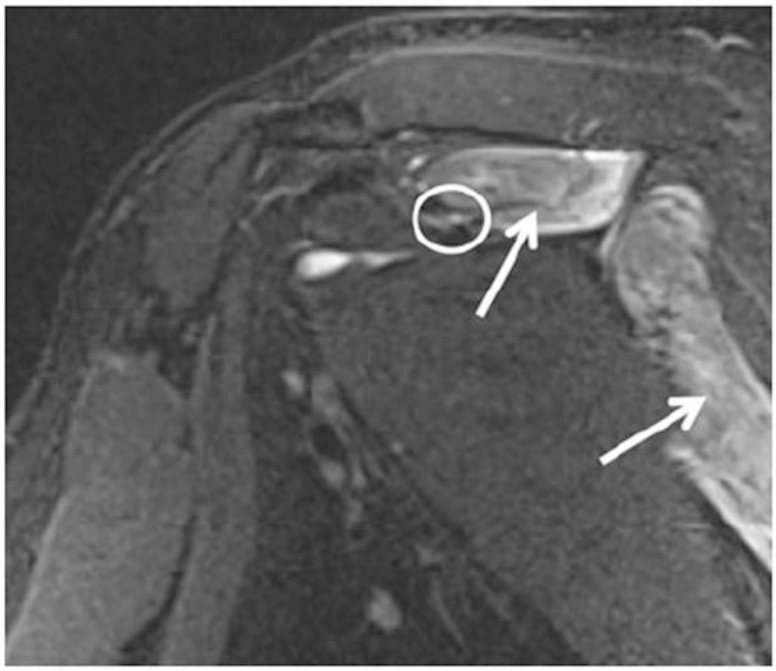

Fig. 11.

A 50-year-old man with shoulder weakness. Sagittal STIR image shows an abnormally hyperintense suprascapular nerve (*encircled*) entrapped at the suprascapular notch, with consequent subacute denervation edema of the supra- and infraspinatus muscles (*arrows*). The patient successfully responded to the suprascapular ligament release. No mass lesion was found intraoperatively

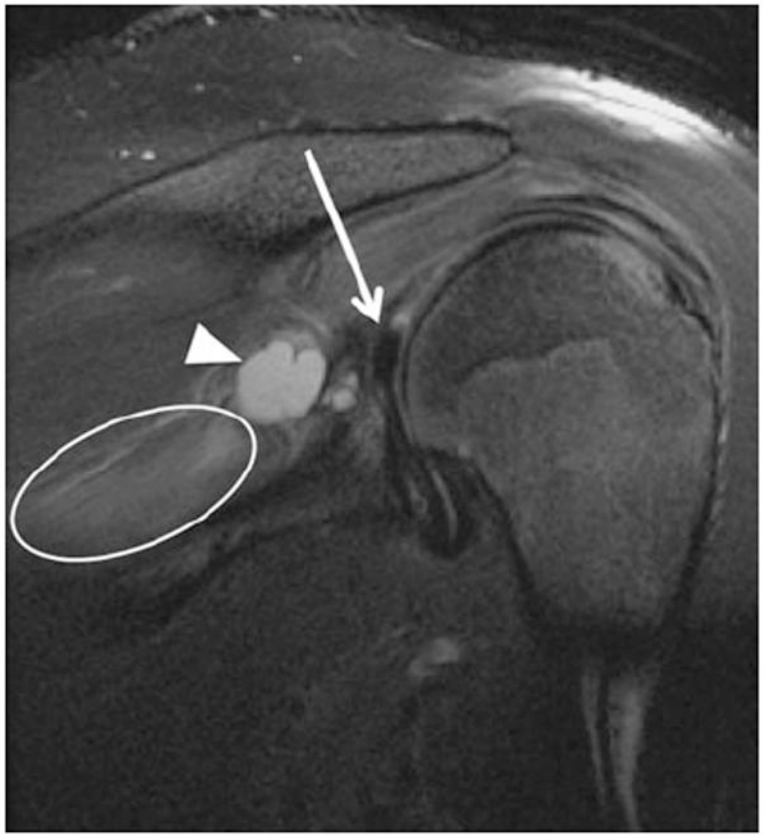

Fig. 12.

A 24-year-old man with shoulder pain and weakness. Coronal proton-density weighted (PDW) image with fat saturation shows a SLAP type II tear (*arrow*), with paralabral cyst formation in the spinoglenoid notch (*arrowhead*), causing entrapment of the supra-scapular nerve and resultant denervation changes of the infraspinatus muscle (*oval*)

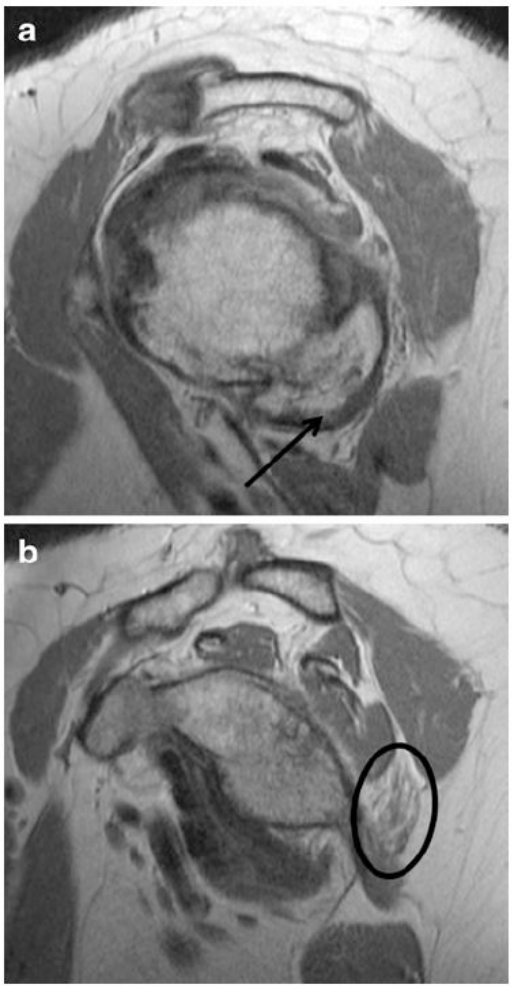

Fig. 13.
A 71-year-old woman with shoulder pain. **a** Sagittal PD images show large humeral osteophytes (*arrow*) projecting into the quadrilateral space. **b** Sagittal PD image medial to **a** shows selective denervation atrophy of the teres minor muscle (*oval*)

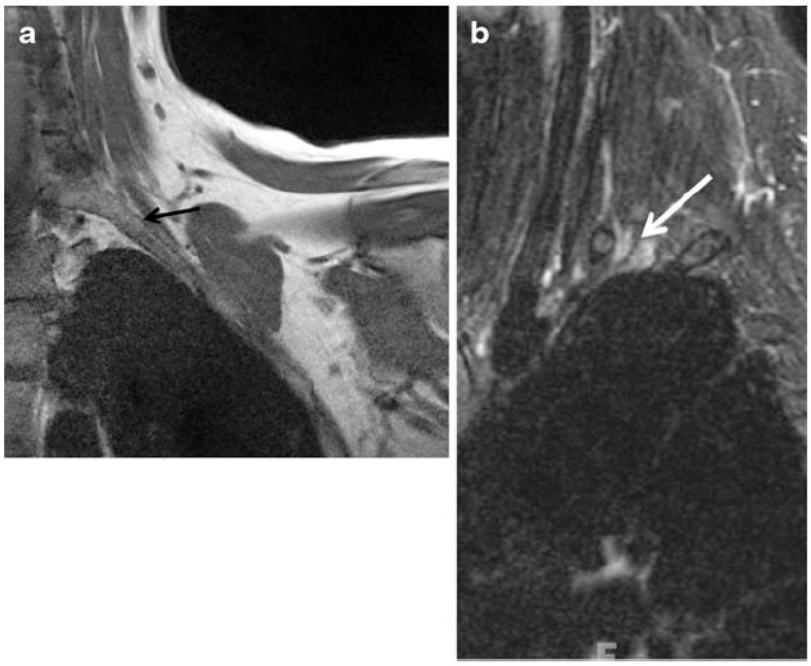

Fig. 14.

A 35-year-old woman with left arm pain. **a** Coronal T1 of the thoracic outlet shows narrowing of the interscalene compartment by a prominent transverse process of C7 (*black arrow*). **b** Sagittal STIR image shows abnormal enlargement and T2 hyperintensity of the C8 and T1 nerve roots (*arrow*), consistent with thoracic outlet syndrome

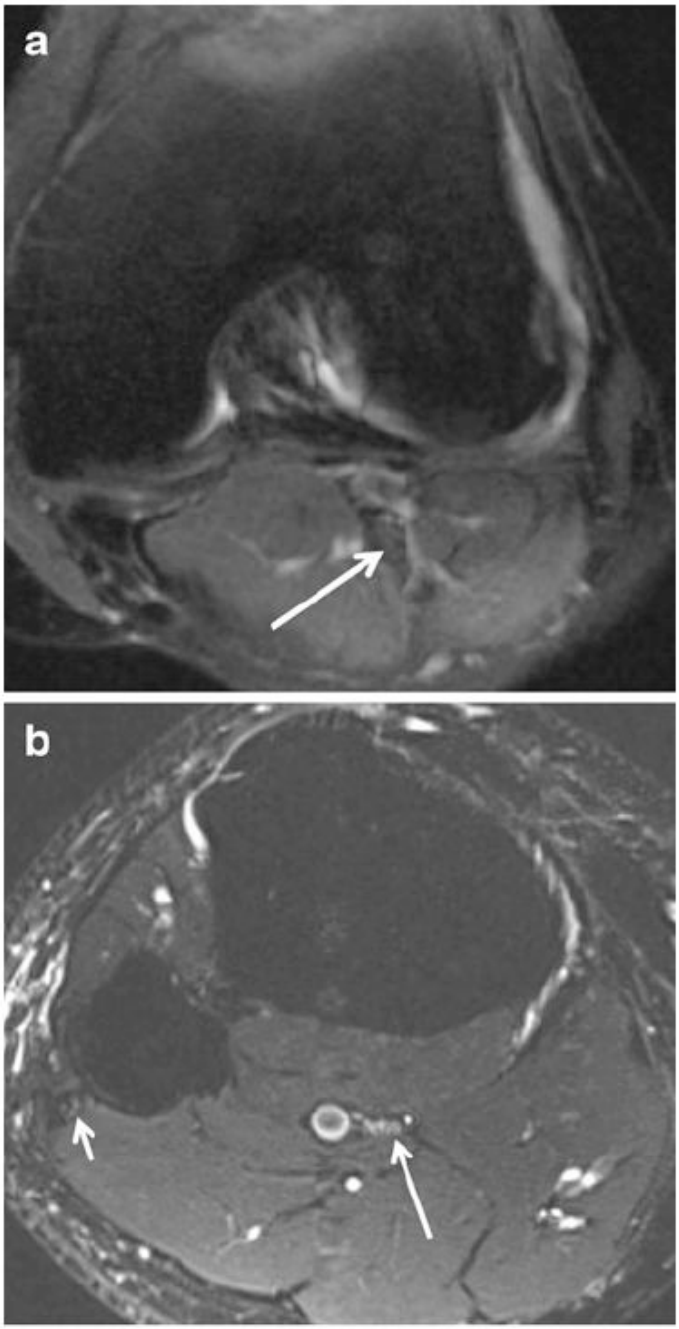

Fig. 15.

A 31-year-old woman with calf pain. **a** Axial T2 SPAIR image shows normal tibial nerve (*arrow*) proximal to the soleal sling. **b** Axial T2 SPAIR image (more distal than **a**) demonstrates subtle hyperintensity of the tibial nerve (*long arrow*) as it crosses under the sling (not well visualized); note normal signal intensity of the common peroneal nerve (*short arrow*). After surgical release of the entrapment, the patient's symptoms improved

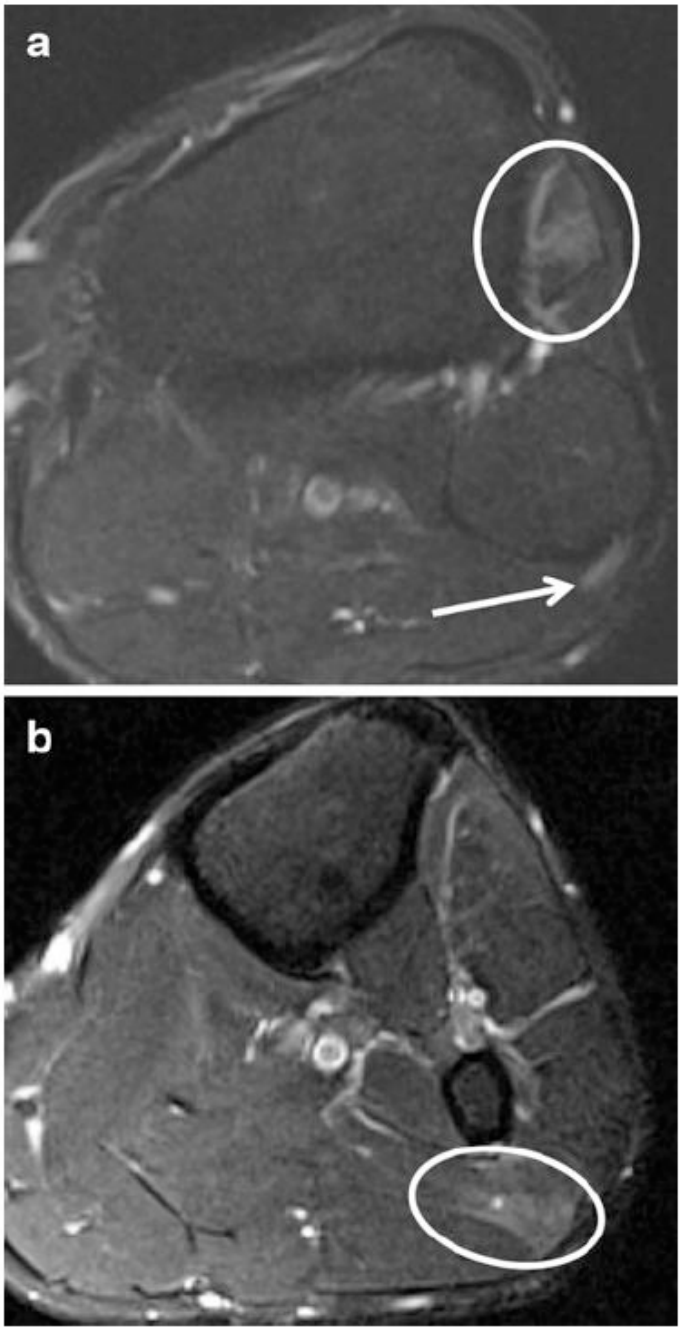

Fig. 16.

A 44-year-old male with left foot drop after sinus surgery, and EMG, which showed evidence of left peroneal neuropathy at the fibular head. **a** Axial T2 SPAIR demonstrates increased signal intensity of the peroneal nerve (*arrow*) posterior to the fibular head in the peroneal tunnel area as well as denervation edema-like signal in the anterior compartment muscles (*encircled*). **b** Axial T2 SPAIR (inferior to **a**) shows grade 1 strain of the lateral head of the gastrocnemius muscle (*encircled*), suggesting local compression due to inattention to proper patient positioning during surgery as the cause of injury

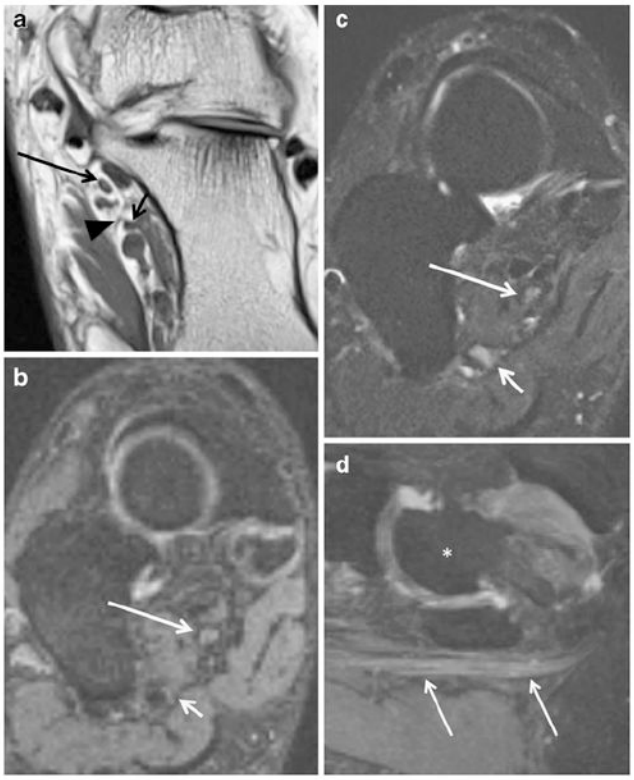

Fig. 17.

A 58-year-old woman with previous tarsal tunnel release and persistent ankle pain in medial plantar nerve distribution. **a** Axial T1 FLAIR demonstrates the medial (*long arrow*) and lateral (*short arrow*) plantar nerves in their respective tunnels; note the thin fibrous septum (*arrowhead*) between the tunnels. **b** Coronal oblique PSIF and **c** SPAIR show subtle increased hyperintensity of the MPN (*long white arrow*) as well as hyperintensity of the LPN (*short white arrow*). **d** Sagittal PSIF MIP shows enlargement of the entrapped MPN (*arrows*); note that vasculature adjacent to the nerves is suppressed on the PSIF images. For orientation, an *asterisk* demarks the talus

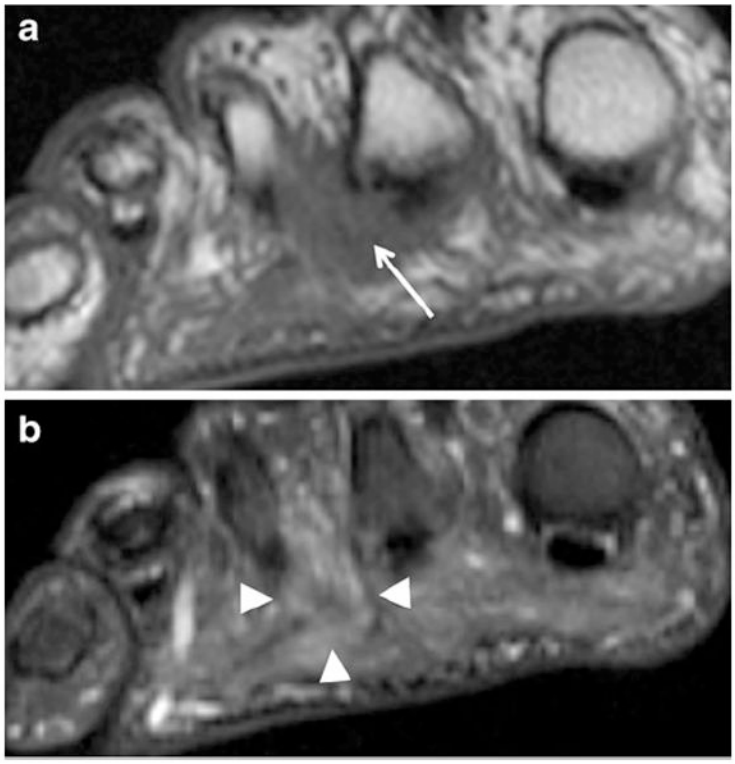

Fig. 18.
A 58-year-old woman with foot pain. Coronal (short-axis axial) T1 image through the distal metatarsals shows intermediate signal intensity mass in the 2nd intermetatarsal web space (*arrow*) with effacement of the fat planes around the common digital nerve. Coronal (short-axis axial) STIR image shows mild hyperintensity within this Morton's neuroma (*arrowheads*)

Table 1

Typical protocol for 3T MR sequences used for MR neurography at the authors' institution. All sequences are run with a small field of view (10–14 cm) and with high-resolution matrix (256×392 or higher)

MR sequence	TR/TE (ms)	Slice thickness	NEX	Flip angle	TF
2-D Axial and coronal T1SE	700–800/9–13	2–3 mm	1	150	6
2-D Axial T2 TSE SPAIR	4,600–7,000/70–80	2–3 mm	1–3	150–180	21–29
3-D T2/STIR SPACE	1,500/97	Isotropic (0.4 mm voxel)	1–2	Variable	123
3-D DW PSIF	10/2.5	Isotropic (0.9 mm voxel)	1	35	–
3-D T1 VIBE	13/5	Isotropic (0.6 mm voxel)	1	10	–

SE Spin echo, *TSE* turbo spin echo, *SPAIR* spectral adiabatic inversion recovery, *SPACE* sampling perfection with application-optimized contrasts using different flip angle evolutions, *STIR* short tau inversion recovery, *DW PSIF* diffusion weighted reversed fast imaging with steady-state precession, *VIBE* volumetric interpolated breath-hold examination, *TR/TE* repetition time/echo time, *NEX* number of averages, *TF* turbo factor (echo train length)

Table 2

Various tunnels in the upper and lower extremities

Tunnel[a]	Nerve
Carpal tunnel	Median
Guyon's canal	Ulnar
Cubital tunnel	Ulnar
Radial tunnel	Radial nerve (± PIN)
Anterior interosseous tunnel	AIN
Suprascapular notch	Suprascapular
Spinoglenoid notch	Suprascapular
Quadrilateral space	Axillary
Thoracic outlet	Various nerves arising from C5–T1
Peroneal tunnel	Peroneal
Soleal sling	Tibial
Tarsal tunnel	Tibial, MPN, and LPN
Plantar tunnels	MPN, LPN, and calcaneal
Intermetatarsal space (Morton's neuroma)	Interdigital

PIN Posterior interosseous nerve, *AIN* anterior interosseous nerve, *MPN* medial plantar nerve, *LPN* lateral plantar nerve

[a] A tunnel is the confined space through which a peripheral nerve normally passes, susceptible to various intrinsic or extrinsic abnormalities that may lead to nerve entrapment and injury